

Weierstraß–Institut für Angewandte Analysis und Stochastik

im Forschungsverbund Berlin e.V.

Inverse problems in optical tomography

Rolf Hünlich¹, Regine Model², Matthias Ortl², Monika Walzel²

submitted: 1st December 1995

¹ Weierstraß–Institut
für Angewandte Analysis
und Stochastik
Mohrenstraße 39
D – 10117 Berlin
Germany

² Physikalisch–Technische
Bundesanstalt
Abbestr. 2–12
D – 10587 Berlin
Germany

Preprint No. 204
Berlin 1995

Edited by
Weierstraß-Institut für Angewandte Analysis und Stochastik (WIAS)
Mohrenstraße 39
D — 10117 Berlin
Germany

Fax: + 49 30 2044975
e-mail (X.400): c=de;a=d400-gw;p=WIAS-BERLIN;s=preprint
e-mail (Internet): preprint@wias-berlin.de

FOREWORD

This preprint contains the revised version of two papers presented at the BiOS Europe '95 held at Barcelona in September 1995 (to appear in Proc. SPIE **2626**). Both papers are devoted to inverse problems in optical tomography. The photon migration in highly scattering media is described by the diffusion equation including some absorption term and by suitable initial and boundary conditions. It represents a good approximation assuming scattering predominates over absorption. Algorithms for solving these inverse problems are an essential part in developing medical diagnostic methods based on transillumination of tissue.

In the first paper

R. MODEL, R. HÜNLICH, Parameter sensitivity in near infrared imaging, pp. 2-11

it is shown that the choice of boundary conditions sensitively affects the photon propagation and the output fluxes at the boundary of the object. A comparison between measurements¹ of the time-resolved transmittance of ps laser pulses and numerical simulations leads to the result, that boundary conditions of the third kind must be used. Besides of the optical parameters the corresponding boundary parameters have been identified using an iteration method in analogy to the image reconstruction algorithm.

The second paper

M. ORLT, M. WALZEL, R. MODEL, Transillumination imaging performance using time domain data, pp. 12-23

is concerned with the question of improving the image reconstruction algorithm itself. Improvements in reconstruction results may be achieved in two ways, first by adapting the detector arrangements and, secondly, by using a regularization strategy based on the Tikhonov regularization. The effectiveness of these methods is demonstrated by instructive examples concerned with the reconstruction of absorbers and scatterers, respectively.

R. Hünlich

¹These measurements were performed by H. RINNEBERG, U. SUKOWSKI, H. WABNITZ, "Medical Measuring Techniques" group of the PTB.

Parameter Sensitivity in Near Infrared Imaging

R. Model^{*}, *R. Hünlich*[†]

^{*}Physikalisch-Technische Bundesanstalt (PTB)
Department of Medical Physics and Information Technology
Abbestraße 2-12, D-10587 Berlin, Germany

[†]Weierstrass Institute for Applied Analysis and Stochastics (WIAS)
Mohrenstraße 39, D-10117 Berlin, Germany

ABSTRACT

To model the photon migration in highly scattering media, we use an approximation of the Boltzmann equation, the diffusion equation. A prerequisite for handling the inverse problem consists in solving the forward problem under realistic conditions. We discuss the influence of boundary conditions on the light propagation. The boundary conditions at the walls surrounding the object highly sensitively influence the photon flux at the boundary which means that the time-resolved transmittance is affected. An algorithm for the determination of boundary parameters is introduced and demonstrated by an instructive example. We use the Finite Element Method for the time-resolved case as a basic method in combination with a minimization strategy. The boundary conditions are determined as conditions of the third kind, i.e. the photon density is proportional to the outward photon flux at the boundary.

1 INTRODUCTION

Reconstruction algorithms for optical imaging are in general based on physical models for the photon migration describing the relation between the measured values and the optical properties of the object under investigation. The propagation of light in highly scattering media, such as biological tissue may be described by the transport theory¹. The Boltzmann equation is in general difficult to solve and too complex for parameter identifications. If the medium is predominantly scattering and sufficiently thick, such that the photons are multiply scattered inside it, the diffusion approximation is a good approach to the Boltzmann equation and widely used in optical tomography. The resulting diffusion equation for the photon density Φ is the following

$$\frac{\partial}{\partial t} \Phi(\mathbf{x}, t) = \operatorname{div}(D(\mathbf{x}) \operatorname{grad} \Phi(\mathbf{x}, t)) - c \mu_a(\mathbf{x}) \Phi(\mathbf{x}, t) + s(\mathbf{x}, t), \quad \mathbf{x} \in \Omega, \quad 0 \leq t \leq T \quad (1)$$

where c is the speed of light in the medium and $\mu_a(\mathbf{x})$ the absorption coefficient. The optical diffusion coefficient $D(\mathbf{x})$ is given by

$$D(\mathbf{x}) = \frac{c}{3(\mu_a(\mathbf{x}) + \mu'_s(\mathbf{x}))} \quad (2)$$

where $\mu'_s(\mathbf{x})$ is the transport scattering coefficient. The light source may be described in two ways, first by the photon source term $s(\mathbf{x}, t)$ in equation (1) and secondly by the initial function $\Phi(\mathbf{x}, 0) = \Phi_0(\mathbf{x})$, $\mathbf{x} \in \Omega$, corresponding to a δ -impulse in time. For ultrashort pulses, the results are approximately the same.

Uniqueness of the solution of (1) is given if suitable conditions at the boundary $\partial\Omega$ are formulated. For the description of light propagation in random media, there are two ways of considering the conditions at the surface. Following the first, it is stated that the walls perfectly absorb the photons hitting them from inside, especially if the walls are black. With the argument that all photons are absorbed at the boundary, the photon density vanishes and homogeneous Dirichlet conditions (boundary conditions of the first kind)

$$\Phi(\mathbf{x}, t) = 0, \quad \mathbf{x} \in \partial\Omega, \quad 0 \leq t \leq T \quad (3)$$

are assumed²⁻⁴. This type is mostly used in reconstruction algorithms, but it seems to be roughly simplified.

A second approach as regards the boundary conditions is derived from Boltzmann's transport equation, in the same way as it is done with the diffusion equation. Here, the diffuse intensity, approximated by the weighted sum of the photon density and the photon flux \mathcal{J} in the outside direction of the medium, must vanish^{1,5,6}. The result is a boundary condition of the third kind

$$\mathcal{J}(\mathbf{x}, t) = -D \frac{\partial \Phi(\mathbf{x}, t)}{\partial n} = h \Phi(\mathbf{x}, t), \quad \mathbf{x} \in \partial\Omega, \quad 0 \leq t \leq T. \quad (4)$$

It can be approximated by theoretically shifting the boundary outward by a small distance and using conditions of the first kind there^{7,8}. If the Finite Element Method (FEM) is applied, boundary conditions of the third kind can be easily realized without such manipulations. For $h = 0$, the flux vanishes or, in other words, a total reflection at the surface is described. This boundary condition is called a condition of the second kind which is independent of the density itself. For $h \rightarrow \infty$, the flux must remain finite, therefore $\Phi(\mathbf{x}, t) = 0$ must be true at the boundary and (4) turns into the condition of the first kind. In reality, $0 < h < \infty$ is valid, but the exact value depends on the experimental setup. The time-resolved transmittance, assumed to be proportional to \mathcal{J} , very sensitively responds to changes at the boundary. It is, however, the input for reconstruction procedures in the case of time-domain imaging. Careful modelling of the situation at the object surface is therefore a prerequisite for handling the inverse problem.

In the next section, the forward simulation for a test structure, i.e. a cuvette containing a diffusely scattering liquid and a movable baffle, is explained. The influence of the boundary parameter h on \mathcal{J} and on some related parameters is shown in section 3. A method for fitting the boundary parameter based on given transmittance is described in section 4 and applied to experimental data. Measurements of the time-resolved transmittance of ps laser pulses were performed by the group "Medical Measuring Techniques" of the PTB using time-correlated single photon counting (for details see⁴). These measurements were performed in a way which allowed a quantitative comparison to be made with the simulations described below.

2 THE FORWARD PROBLEM

The diffusion equation (1) is solved by a 2D FEM with adaptive grid refinement and time step size control which is an effective tool, in particular for complicated geometries and arbitrary distributions of the optical properties.

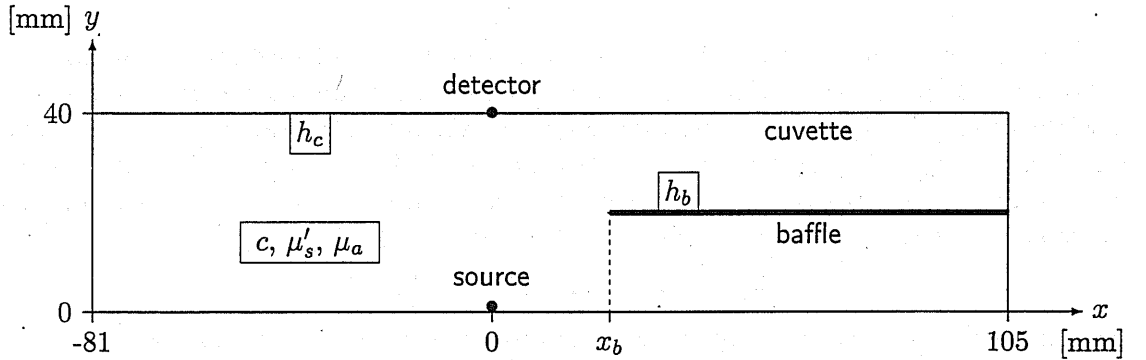


Fig. 1. Test structure. The source position is $x_s = 0$ mm, $y_s = 1$ mm, the detector position is $x_d = 0$ mm, $y_d = 40$ mm, the left position of the baffle x_b is variable. Indicated are the physical parameters c , μ'_s , μ_a describing the properties of the homogeneous medium inside the cuvette, and h_c , h_b describing the absorption and reflection properties of the wall of the cuvette and of the baffle, respectively.

In Fig. 1, the test structure is illustrated which is a cross section of a rectangular cuvette with a movable baffle inside. The parameters h_c , h_b of the boundary conditions

$$\begin{aligned} -D \frac{\partial \Phi(\mathbf{x}, t)}{\partial n} &= h_c \Phi(\mathbf{x}, t) && \text{on the wall of the cuvette,} \\ -D \frac{\partial \Phi(\mathbf{x}, t)}{\partial n} &= h_b \Phi(\mathbf{x}, t) && \text{on the baffle} \end{aligned} \quad (5)$$

may be different. In the following example of a forward simulation we use the optical parameters⁴

$$c = 22.56 \text{ cm ns}^{-1}, \mu_a = 0.0308 \text{ cm}^{-1}, \mu'_s = 9.15 \text{ cm}^{-1}.$$

The boundary parameters h_c and h_b are both set to 7.5 cm ns^{-1} . The ultrashort pulse is modeled by the initial condition

$$\Phi_0(x, y) = C_s d(x, y), \quad d(x, y) = \begin{cases} 1 & \text{if } \sqrt{(x - x_s)^2 + (y - y_s)^2} < r_s \\ 0 & \text{else} \end{cases}$$

setting $C_s = 10^6 \text{ cm}^{-3}$, $r_s = 0.1$ mm. For the same structure, simulations were done earlier with homogeneous Dirichlet conditions⁴.

Resulting surface plots of the photon density for different times ($t=0.2, 0.5, 1.0, 2.0, 3.0, 4.0$ ns) are given in Fig. 2. Note that each of the plots is normalized to the maximum density of the actual time which quickly decreases as indicated explicitly. It is clearly visible that the light turns around the baffle depending on time.

Fig. 3 shows isolines of the photon density for $t = 2$ ns and, in addition, the source position and six detector positions (detector 5 corresponds to the only detector in Fig. 1) for which the photon densities are compared in Fig. 4. As expected, the influence of the baffle is most remarkable for detector 6 which is reached by the smallest number of photons. However, there is also an effect on the densities at the other detector positions. Because boundary conditions of the third kind were used, the density is proportional to the photon flux and therefore to the diffuse transmittance.

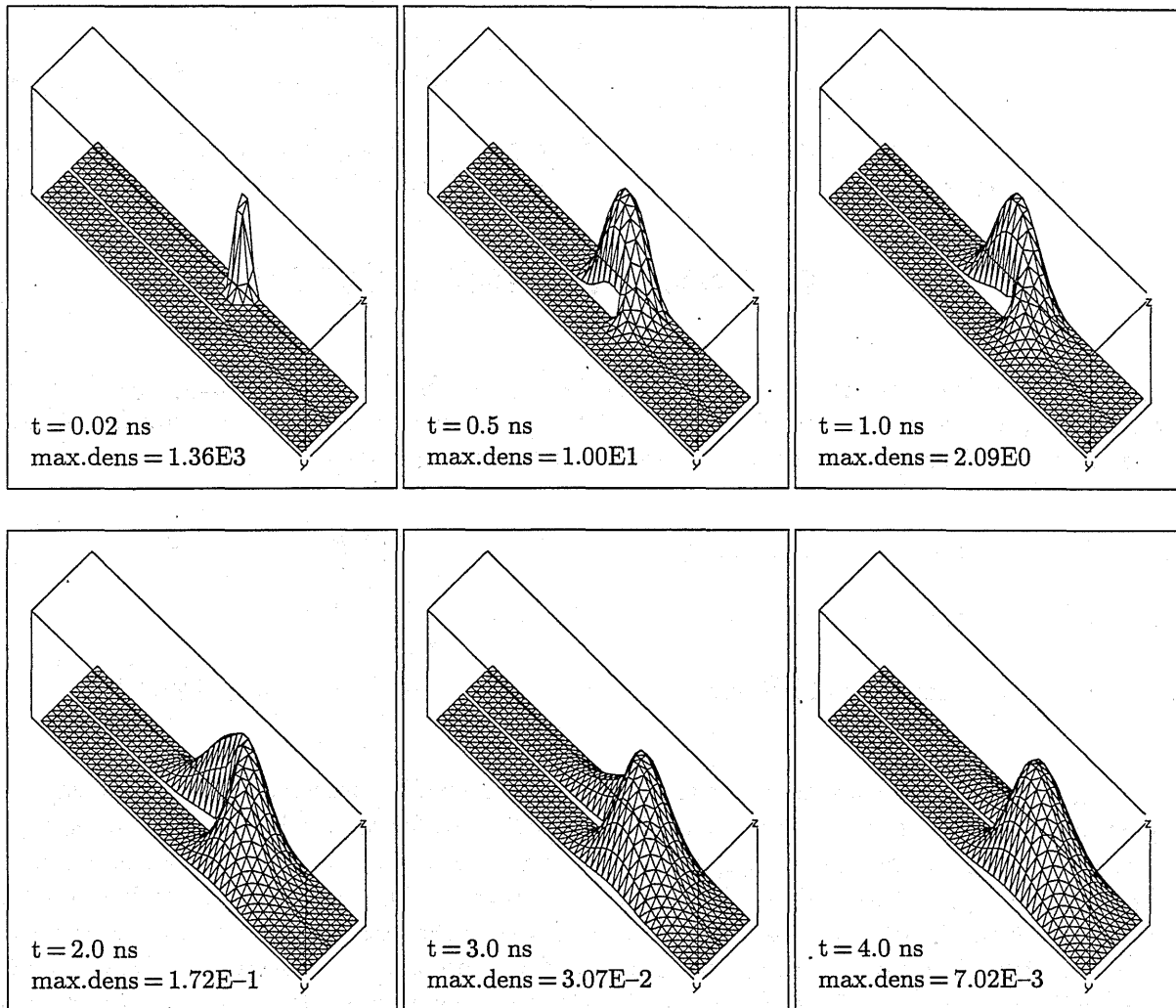


Fig. 2. Light propagation depending on time. Here the photon density surface is seen from the detector side such that the baffle is located on the left-hand side. The baffle position is $x_b = -6$ mm.

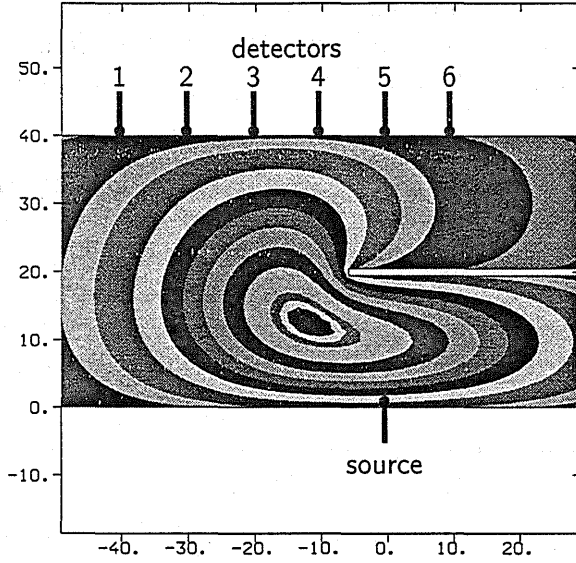


Fig. 3. Photon density in the cross section of the cuvette for $t = 2.0$ ns.

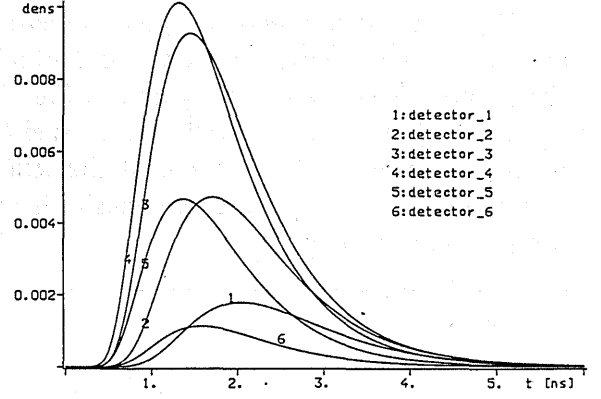


Fig. 4. Photon density [cm^{-3}] as a function of time at various detector positions.

3 PARAMETER SENSITIVITY

Now the influence of the boundary parameters h_c and h_b on the light propagation inside the cuvette and on the photon density at some detector position as a function of time is discussed. We use the following characteristics of these photon density curves:

$$\begin{aligned}
 I_{max} &= \text{max. of photon density}, & I_{tot} &= \int_0^{\infty} \Phi(t) dt, \\
 t_{max} &= \text{time realizing } I_{max}, & t_{mean} &= \frac{1}{I_{tot}} \int_0^{\infty} t \Phi(t) dt, \\
 t_{half} &= \text{full width of half max.}, & \sigma &= \left[\frac{1}{I_{tot}} \int_0^{\infty} (t - t_{mean})^2 \Phi(t) dt \right]^{1/2}.
 \end{aligned}$$

Fig. 5 shows these characteristics as a function of the baffle position x_b (from the most closed position at -15 mm to the widest open position at 36 mm) for some selected values of h_c and h_b where the other parameters c , μ_a , μ'_s remain unchanged as above. Source and detector are chosen as shown in Fig. 1. Case 1 (with $h_c = h_b = 10 \frac{c}{3}$) corresponds approximately to the boundary condition of the first kind. Case 2 (with $h_c = h_b = \frac{c}{3}$) is the most realistic one, in cases 3 and 4 the reflection increases. Case 5 and 6 consider different boundary parameters on the wall and on the baffle, respectively. For example, in all cases the maximum value I_{max} decreases when the baffle is moved to more closed positions. In the case with the highest reflection, the maximum values are largest (curve 4) as expected. When the baffle's influence becomes greater, curve 6 differs from curve 4 due to the changed parameter h_b . In general, the influence of the baffle appears clearer at the higher moments. Note that t_{max} , t_{mean} , t_{half} and σ have a minimum at a baffle position between 0 mm and 5 mm.

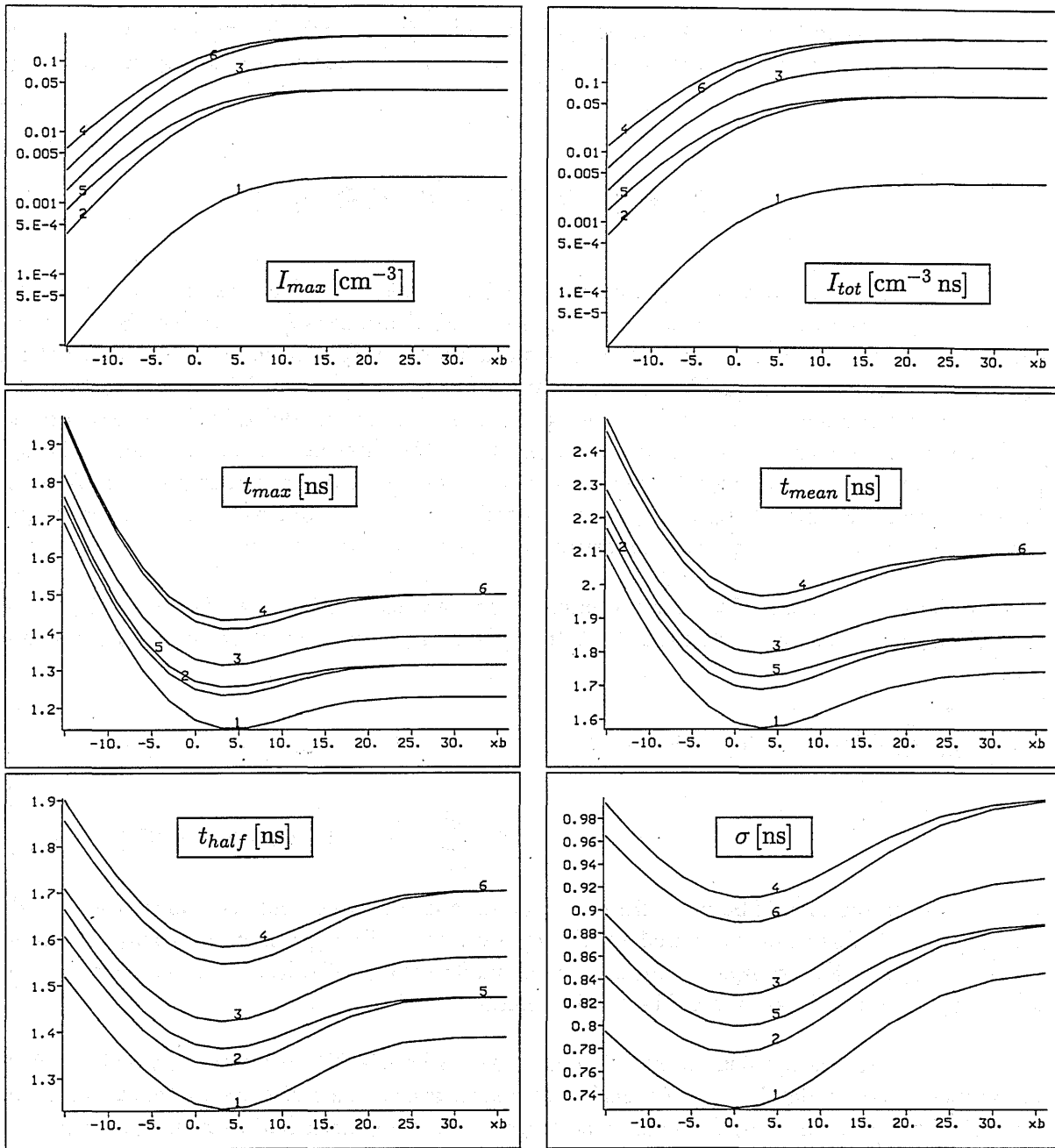


Fig. 5. Variation of the boundary parameters h_c, h_b [cm ns^{-1}] and of the baffle position x_b [mm]. The following values of h_c, h_b have been used:

- case 1: $h_c = 75.2$ $h_b = 75.2$
- case 2: $h_c = 7.52$ $h_b = 7.52$
- case 3: $h_c = 3.76$ $h_b = 3.76$
- case 4: $h_c = 1.88$ $h_b = 1.88$

- case 5: $h_c = 7.52$ $h_b = 1.88$
- case 6: $h_c = 1.88$ $h_b = 7.52$.

From this it follows that the boundary parameters highly sensitively affect all characteristics. The solution of reconstruction problems therefore seems to require a reliable knowledge of the boundary parameters.

4 THE INVERSE PROBLEM

At first sight, the two parameters in the boundary conditions (5) for cuvette h_c and baffle h_b must be fitted. However, the optical properties μ_a and μ'_s are usually determined by comparing experimental data with an analytical approximation for the solution of (1) using Dirichlet conditions in a bounded domain^{2,9}. For boundary conditions of the third kind (4), an analytical solution in a bounded domain is not on hand, so μ_a and μ'_s are included in the inverse problem as unknown parameters. Furthermore, sometimes the absolute number of photons of the laser pulse entering the object and the exact start time of the pulse are not known either. A scaling factor Φ_I and a time shift t_{sh} are therefore added to the set of unknowns. In addition, a given response function of the experimental setup must be taken into account.

For the identification of the six parameters, an iteration method was developed in analogy to the image reconstruction method^{4,9-11}. It is based on the minimization problem of the error norm

$$\begin{aligned} \sum_{k=1}^p \sum_{i=1}^n |\mathcal{J}^s(x_{b_i}, t_k, h_c, h_b, \mu_a, \mu'_s, \Phi_I, t_{sh}) - \mathcal{J}^m(x_{b_i}, t_k)|^2 \\ = \sum_{s=1}^{np} |F_s(h_c, h_b, \mu_a, \mu'_s, \Phi_I, t_{sh})|^2 = \min! \end{aligned} \quad (6)$$

where n is the number of baffle positions, p the number of times, and the supercripts s and m denote the simulated and measured values, respectively. The algorithm can easily be adapted to other objects, for example to those without baffle inside. The least squares problem (6) is solved by a modified Levenberg–Marquardt–Method.

The method was applied to experimental data, where a 2D situation was realized in the experiment (see for details^{4,12}). An earlier comparison between these experimental results and numerical simulations using Dirichlet conditions at the boundaries had furnished unsatisfactory results⁴. Even by a new identification of the parameters μ_a , μ'_s , Φ_I and t_{sh} according to (6) (the dependence on h_c , h_b is cancelled here), better agreement could not be achieved as can be seen in Fig. 6. Note that a single curve normalized to its maximum compared with the corresponding measurement data normalized to their maximum has led to good results. However, for more than one baffle position, a comparison is impossible.

Now, boundary conditions of the third kind are applied. Here six parameters including h_c , h_b have been identified according to (6). Excellent agreement is achieved as shown in Fig. 7. h_c is greater than h_b which suggests that the baffle reflects the light more than does the wall of the cuvette. But the uncertainty is estimated at about ten per cent, because the problem is bad conditioned and has a flat minimum. Higher precision may be reached when reliable values

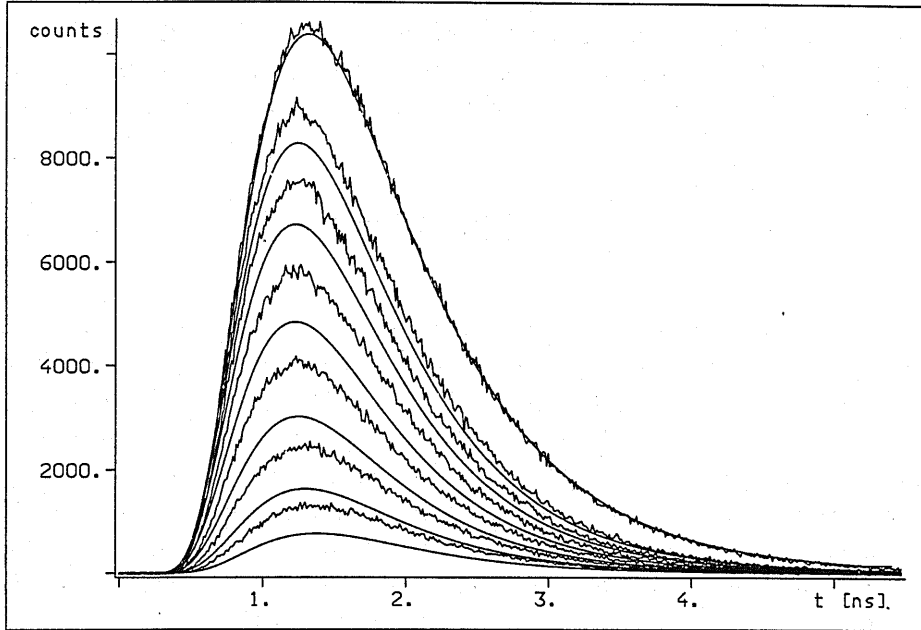


Fig. 6. Measured and computed transmittance for different positions of the baffle ($x_b = 36, 9, 6, 3, 0, -3, -6$ mm from top to bottom) using boundary conditions of the first kind. Optimal values: $\mu_a = 0.028 \text{ cm}^{-1}$, $\mu'_s = 8.96 \text{ cm}^{-1}$.

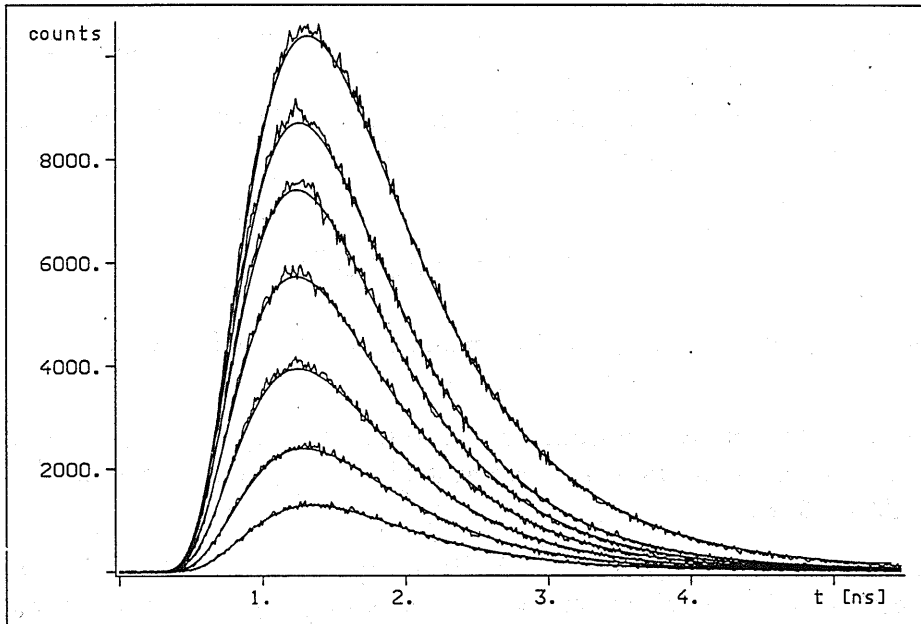


Fig. 7. Measured and computed transmittance for different positions of the baffle ($x_b = 36, 9, 6, 3, 0, -3, -6$ mm from top to bottom) using boundary conditions of the third kind. Optimal values: $\mu_a = 0.028 \text{ cm}^{-1}$, $\mu'_s = 8.1 \text{ cm}^{-1}$, $h_c = 8.99 \text{ cm ns}^{-1}$, $h_b = 6.83 \text{ cm ns}^{-1}$.

of the optical parameters μ_a , μ'_s are used which have been independently determined. Finally, mention should be made of the fact that the identification results are clearly influenced by the given response function. Some questions arise here which require further investigations.

5 CONCLUSIONS

The question about the correct determination of the boundary conditions in optical imaging problems using the diffusion theory may be answered by a constructive method which allows the boundary parameters to be determined as well. The assumption of the photon density's vanishing at the boundary did not furnish a satisfactory result. The excellent agreement between experimental and simulated data in the case of boundary conditions of the third kind strongly suggests the application of this condition. Corresponding to the experimental data, optimal boundary parameters are found which are different for the glass wall and the metal baffle. This shows that the parameters also depend on the experimental setup. A reconstruction of spatially dependent optical properties must therefore include the determination of the boundary parameters. Because of the ill posedness of the resulting numerical problem, these parameters should be obtained by an independent reference measurement avoiding convergence difficulties in the reconstruction procedure itself.

ACKNOWLEDGEMENTS

We would like to thank H. Wabnitz, U. Sukowski and H. Rinneberg of the PTB for providing the experimental data and for helpful discussions.

This work was supported by the German Federal Ministry of Education and Research (BMBF) project number 13N6307.

REFERENCES

- [1] A. ISHIMARU, Wave propagation in random scattering media. Academic Press, New York (1978).
- [2] M. S. PATTERSON, B. CHANCE, B. C. WILSON, Time-resolved reflectance and transmittance for the noninvasive measurement of tissue optical properties. *Appl. Optics*, **28**, 2331-2336 (1989).
- [3] S. R. ARRIDGE, M. SCHWEIGER, M. HIRAOKA, D. T. DELPY, Performance of an iterative reconstruction algorithm for near-infrared absorption and scatter imaging. *Proc. SPIE* **1888**, 360-371 (1993).
- [4] R. MODEL, R. HÜNLICH, D. RICHTER, H. RINNEBERG, H. WABNITZ, M. WALZEL, Imaging in random media: Simulating light transport by numerical integration of the diffusion equation. *Proc. SPIE* **2326**, 11-22 (1995).

- [5] F. LIU, K. M. YOO, R.R. ALFANO, How to describe the scattered ultrashort laser pulse profiles measured inside and at the surface of a random medium using the diffusion theory. Proc. SPIE 1888, 103-106 (1993).
- [6] C. P. GONATAS, M. MIWA, M. ISHII, J. SCHOTLAND, B. CHANCE, J. S. LEIGH, Effects due to geometry and boundary conditions in multiple light scattering. Proc. SPIE 1888, 402-406 (1993).
- [7] R. ARONSON, Extrapolation distance for diffusion of light. Proc. SPIE 1888, 297-305 (1993).
- [8] L. O. SVAASAND, D. HASKELL, B. TROMBERG, M. MCADAMS, Properties of photon density waves at boundaries. Proc. SPIE 1888, 214-226 (1993).
- [9] R. MODEL, R. HÜNLICH, M. ORLT, M. WALZEL, Image reconstruction for random media by diffusion tomography. Proc. SPIE 2389, 400-410 (1995).
- [10] R. MODEL, R. HÜNLICH, Optical imaging of highly scattering media. ZAMM (1996). In press.
- [11] M. ORLT, M. WALZEL, R. MODEL, Transillumination imaging performance using time domain data. This volume.
- [12] H. WABNITZ, R. WILLENBROCK, J. NEUKAMMER, U. SUKOWSKI, H. RINNEBERG, Spatial resolution in photon diffusion imaging from measurements of time-resolved transmittance. Proc. SPIE 1888, 48-61 (1993).

Transillumination imaging performance using time domain data

M. Orlt, M. Walzel, R. Model

Physikalisch-Technische Bundesanstalt,
Department of Medical Physics and Information Technology,
Abbestraße 2-12, D-10587 Berlin, Germany

ABSTRACT

Light propagation in highly scattering media can be numerically simulated by solving the diffusion equation by the Finite Element Method (FEM). Employing an iterative algorithm, the FEM solution of the forward problem is applied to the inverse imaging problem. Good test results were previously achieved when absorbers were searched in different objects. Now the reconstruction of scattering is also taken into account. Simulated measurement data are used to test and evaluate the method at various objects with tissue-like properties. Resulting problems are very ill posed. The algorithm is specially adapted to the illposedness of the problem. Improvements in reconstruction results can be achieved in two ways, first by adapting the detector arrangements and, secondly, by using a regularization strategy. The effectiveness of these methods is demonstrated by instructive examples.

1 INTRODUCTION

When a laser light pulse is sent through tissue, the spatial and time-resolved measurement of the output flux contains some information about the inner distribution of optical parameters.^{2,5,11-13} Light propagation in highly scattering media can be described by the diffusion theory.⁶ The inverse imaging problem of the optical tomography then appears as a parameter identification problem of a partial differential equation. As there are effective numerical tools to solve the diffusion equation even for inhomogeneous objects, for example the Finite Element Method (FEM), we include it for application to the inverse problem.^{8,9}

However, parameter identification problems are ill posed in most cases, meaning that large differences of the optical parameters cause only small differences in the measured or simulated output flux. Basic numerical methods are known to handle such problems, but a lot of detailed investigations are needed to apply them to the inverse imaging problem of optical tomography. Algorithms must be developed which can use the full information contained in a spatial and time-resolved measurement.

The algorithm is tested using simulated measurement data computed for 2D objects, several centimeters in size and with tissue-like optical parameters. The performance of the reconstruc-

tion algorithm is demonstrated by the fact that absorbers and scatterers of small dimensions (several millimeters) and small parameter deviations (4–10 times of the underground) are found in these test objects.

2 MATHEMATICAL MODEL

With certain restrictions which apply to the present problem, light propagation can be described by the diffusion theory.⁶ In this case, the solution of a parabolic differential equation

$$\frac{\partial}{\partial t} \Phi(\mathbf{x}, t) - \text{div} (D(\mathbf{x}) \text{grad} \Phi(\mathbf{x}, t)) + c\mu_a(\mathbf{x})\Phi(\mathbf{x}, t) = s(\mathbf{x}, t), \quad (\mathbf{x}, t) \in \Omega \times (0, T) \quad (1)$$

provides the spatial and time-dependent photon density $\Phi(\mathbf{x}, t)$ in the object investigated. μ_a and μ'_s are the spatially dependent optical parameters of absorption and reduced scattering. The optical diffusion coefficient $D(\mathbf{x})$ is related to $\mu_a(\mathbf{x})$ and $\mu'_s(\mathbf{x})$ by the equation

$$D(\mathbf{x}) = \frac{c}{3(\mu_a(\mathbf{x}) + \mu'_s(\mathbf{x}))} \quad (2)$$

The initial condition $\Phi(\mathbf{x}, 0) = \Phi_0(\mathbf{x})$ for a known photon distribution $\Phi_0(\mathbf{x})$ at the time $t = 0$ and the boundary condition

$$D(\mathbf{x}) \frac{\partial \Phi}{\partial \mathbf{n}}(\mathbf{x}, t) + h\Phi(\mathbf{x}, t) = 0, \quad (\mathbf{x}, t) \in \partial\Omega \times (0, T) \quad (3)$$

complete the mathematical formulation of the forward model. The boundary condition of the third kind (3) is derived applying the diffusion approximation to the general boundary condition of Boltzmann's transport equation stating that no diffuse intensity enters the medium from outside.^{6,7} The constant h depends on the speed of light c and the experimental setup and should be determined in advance by a reference measurement and a parameter identification procedure.¹⁰ The output photon flux

$$J(\mathbf{x}, t) = -D(\mathbf{x}) \frac{\partial \Phi}{\partial \mathbf{n}}(\mathbf{x}, t) \Big|_{\partial\Omega} \quad (4)$$

is assumed to be proportional to the time-resolved measurements.

The Finite Element Method is an effective numerical tool to solve the problem (1)–(4) even for inhomogeneous distributions of the optical parameters and for complicated geometries and boundary conditions. On the basis of a discretization in space and time, the unknown photon density is approximated by a piecewise linear function.⁸ Figure 1 shows an example of the discretization of a rectangular object. Because of the large gradients of the photon density in a first short time interval, an additional refinement is necessary to achieve an appropriate accuracy of the numerical simulation.

In the inverse imaging algorithm, the (given) measured information about the time-resolved transmittance $\mathbf{J}^{mes} = (J_1^{mes}(\mathbf{x}_{11}, t_{11}), \dots, J_i^{mes}(\mathbf{x}_{ij}, t_{ijk}), \dots)$ is used. The subscripts i, j, k indicate the actual source, detector and time respectively such that one entry of the measurement vector $J_i^{mes}(\mathbf{x}_{ij}, t_{ijk})$ is the photon flux which can be detected at the position \mathbf{x}_{ij} and the time

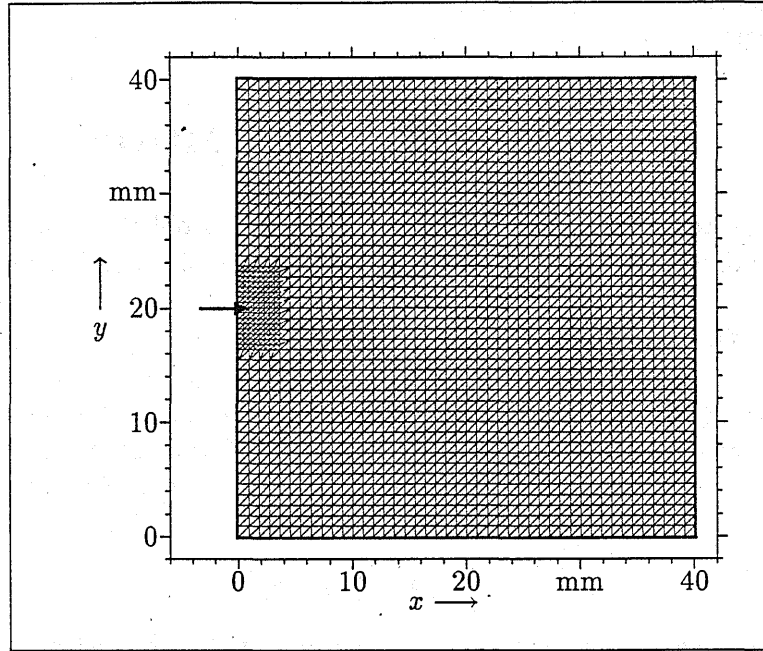


Figure 1: FEM grid for the solution of the forward problems within the reconstruction algorithm.

t_{ijk} if the source distribution $\Phi_{0i}(\mathbf{x})$ has been applied to the object. This notation allows the number of detectors and the detector positions to be chosen separately for each source and different times to be taken into account for each detector.

The model (1)–(4) and its numerical solution allow a corresponding vector $\mathbf{J}^{sim}(\mu_a, \mu'_s)$ to be simulated on the assumption that $\mu_a(\mathbf{x})$ and $\mu'_s(\mathbf{x})$ are the actual spatially dependent optical parameters of the object. The goal now is to find such $\mu_a(\mathbf{x})$ and $\mu'_s(\mathbf{x})$ which well fit the simulated data $\mathbf{J}^{sim}(\mu_a, \mu'_s)$ to the measured data \mathbf{J}^{mes} . The basic strategy of the fit consists in an iterative correction of the optical parameters and can be demonstrated in a formal procedure:

1. Choose a start approximation μ_a and/or μ'_s .
2. Solve the forward problem, i.e. compute $\mathbf{J}^{sim}(\mu_a, \mu'_s)$.
3. Compare $\mathbf{J}^{sim}(\mu_a, \mu'_s)$ and \mathbf{J}^{mes} ,
if $\|\mathbf{J}^{sim}(\mu_a, \mu'_s) - \mathbf{J}^{mes}\| < \epsilon$ then go to 5.
4. Correct μ_a and/or μ'_s go to 2.
5. end

With the choice of the l_2 -norm to compare the vectors of simulated and measured data, the optimization problem (5) becomes a least squares problem.

$$\|\mathbf{J}^{sim}(\mu_a, \mu'_s) - \mathbf{J}^{mes}\|^2 = \sum_{i=1}^l \sum_{j=1}^{m_i} \sum_{k=1}^{n_{ij}} |J_i^{sim}(\mathbf{x}_{ij}, t_{ijk}, \mu_a, \mu'_s) - J_i^{mes}(\mathbf{x}_{ij}, t_{ijk})|^2 = \min! \quad (6)$$

In this paper, μ_a and μ'_s have been set piecewise constant on a special rectangular grid (see Fig. 2) which must be interpolated to the FEM grid. As expected, this inverse problem is very ill-conditioned. Large differences of the optical parameters cause only small differences in the simulated output flux. This behaviour will be demonstrated in Figures 3–5. The implementation of the Levenberg-Marquardt-Method from the IMSL program library was used to solve the optimization problem (6). Because of its trust region approach³ it is appropriate to handle badly conditioned problems.

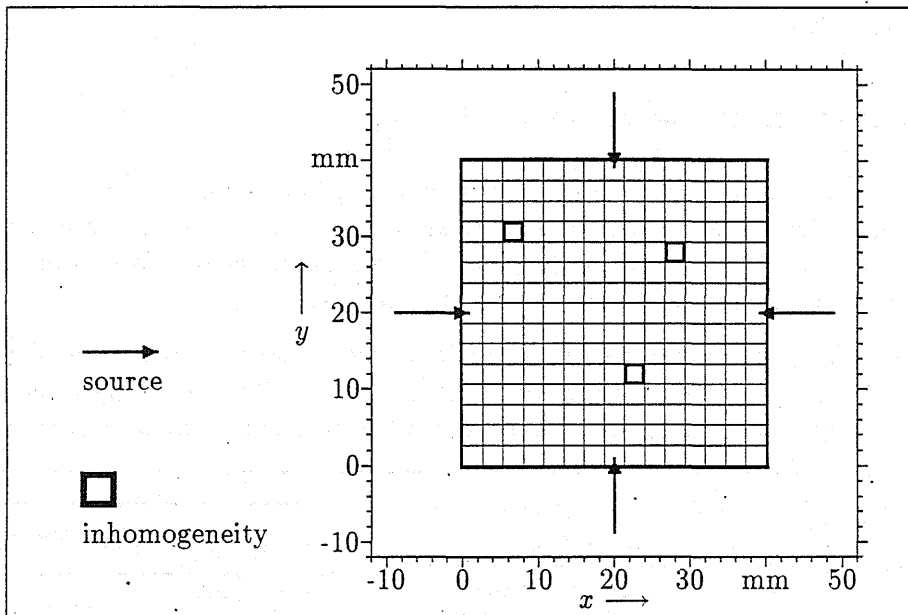


Figure 2: Grid of the setup for the optical parameters μ_a and/or μ'_s and source distribution used for the numerical tests.

Both numerical tools, the FEM code and the Levenberg-Marquardt algorithm for solving the forward and the inverse problem, respectively required a lot of modifications and adaptations of parameters when these methods were applied to the imaging problem. Many numerical tests had therefore to be done before the following results were achieved.

3 RECONSTRUCTION RESULTS

3.1 Test object and measurement simulation

A two-dimensional rectangle with a size of $4\text{cm} \times 4\text{cm}$, an underground absorption of $\mu_a = 0.033\text{cm}^{-1}$ and a reduced scattering of $\mu'_s = 10\text{cm}^{-1}$ served as a test object. We approximated the absorption or the reduced scattering on a rectangular grid with a pixel size of 2.67mm .

For the test object and given inhomogeneities, the forward problem is solved in order to get the time-resolved transmittance as a quasi measurement. The iterative reconstruction procedure begins using constant optical parameters as the initial approximation and the quasi measurement data as the input. In this way a step-by-step approach to the difficulties of imaging from real measurement data is possible.

Two ways of improving the algorithm are discussed in our paper. The first strategy consists in finding an appropriate measurement configuration. Four sources are located at the respective middle point of the boundary pieces and moved into the object at a distance of 1mm (Fig. 2) corresponding to the mean free path length. The aim is to determine a detector arrangement and times for a good detection of inhomogeneities. The second way is the application of a regularization method.

3.2 Arrangement of sources and detectors

In this section the influence of the detector arrangement on the reconstruction result is demonstrated by examples, and a method is presented to improve the detector arrangement. The basic idea is to use as much as possible of the measurement information available while taking into account as few measurement data as possible.

First we set a start configuration (A) (32 detectors per source), where the detectors are distributed equidistantly on the boundary of the object (Fig. 3 right), and apply the reconstruction algorithm. The right side of Figure 3 shows the reconstruction result as a grey level picture. It

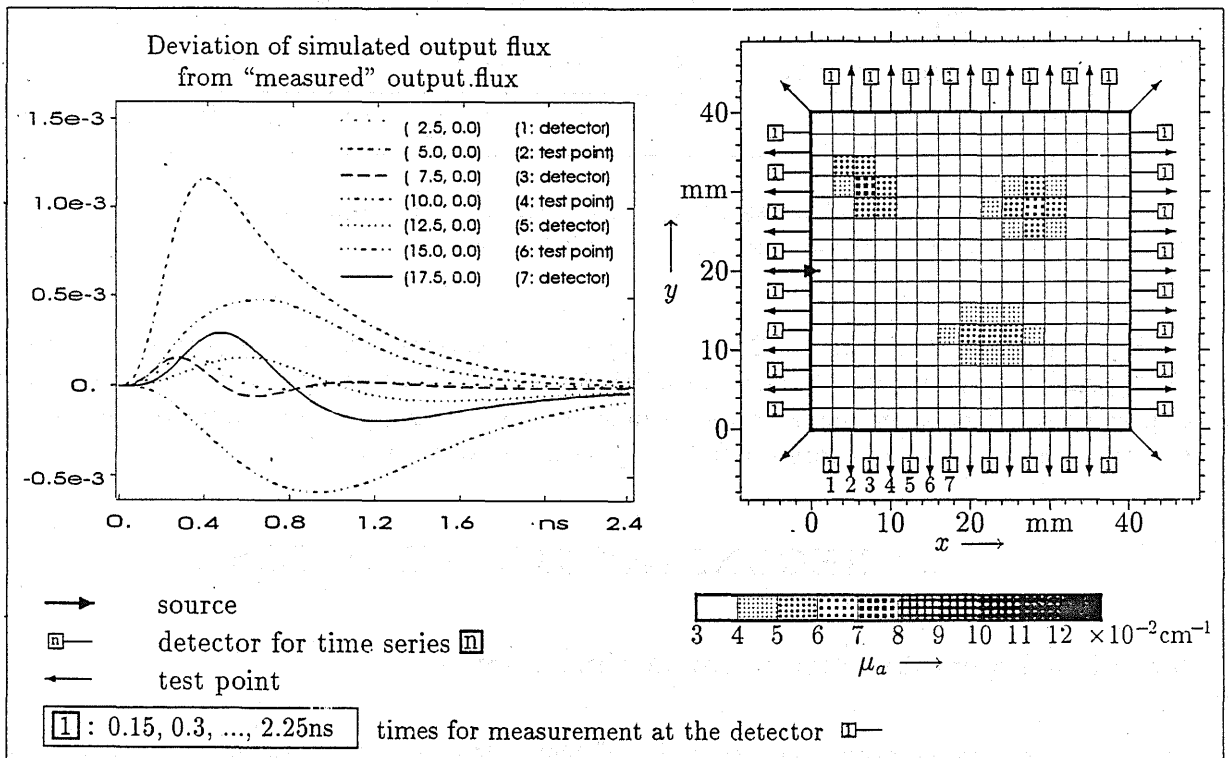


Figure 3: Arrangement (A) of detectors and reconstruction result after 6 iterations.

has been achieved with this detector arrangement (A). In the example, the structure contains 3 absorbers (Fig. 2) $2.67\text{mm} \times 2.67\text{mm}$ in size, with an absorption coefficient $\mu_a = 0.165\text{cm}^{-1}$ (5 times the underground).

Using the reconstruction result, we simulate the output flux in additional test points between the detectors and compare it with the corresponding additional quasi measurement data. In other words, we test whether or not the simulated transmittance of the reconstruction result is fitted to the "measurement" data in additional test points, too. Fig. 3 shows this investigation for one of four sources at the position $x = 1.0, y = 20.0$ and the detectors and test points on the lower left side of the right illustration. The numbers 1–7 at the detectors and test points on the right side refer to the difference curves on the left side of the figure. These curves are normalized using the maximum of output flux at the detector denoted by 1.

If the differences between the output flux of the test object and the reconstructed structure are considerably higher in the test points (curves 2, 4, 6 in Fig. 3 left) compared with those in the previous detector points (curves 1, 3, 5, 7 in Fig. 3 left), it can be assumed that there is some measurement information available at these test points, which has not yet been used in the reconstruction. It may be expected that additional detectors in such regions can provide more information and improve the reconstruction result. On the other hand, in regions where the deviations between the simulated and measured transmittance in the test points are small, detectors can be removed.

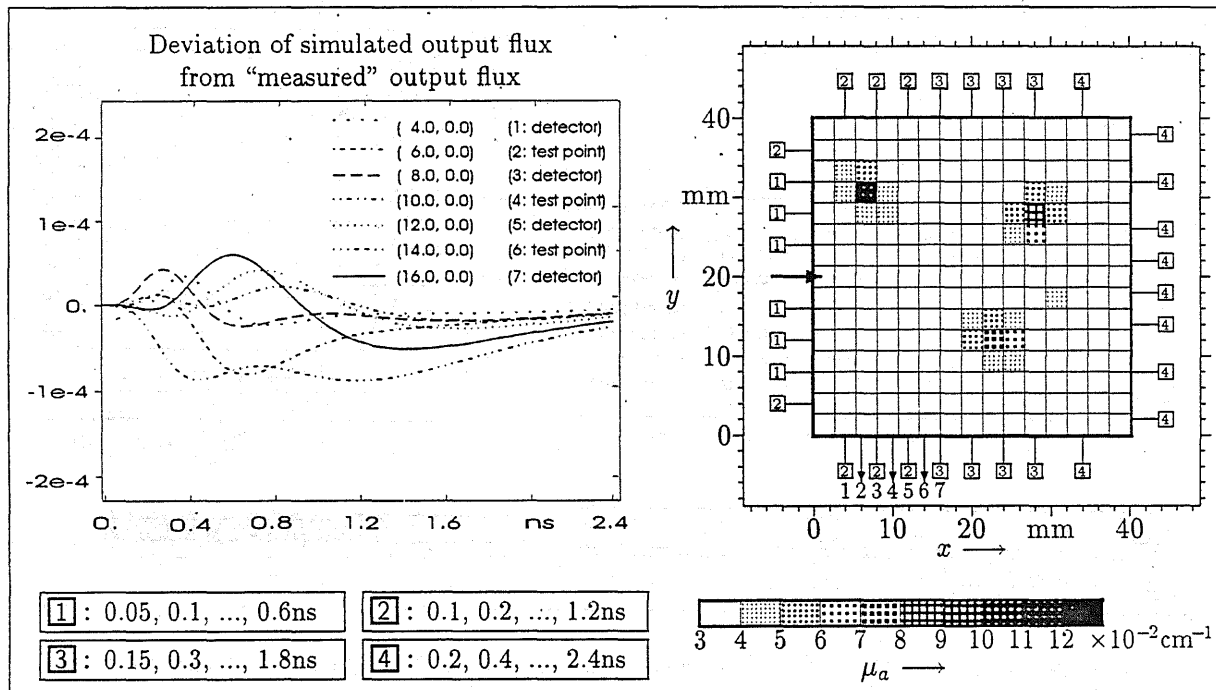


Figure 4: Arrangement (B) of detectors and reconstruction result after 6 iterations.

The described correction of the detector arrangement leads to configuration (B). As expected, this arrangement provides a better reconstruction result (see Figure 4). This configuration could be tested by repeating the procedure suggested above. It is summarized in the following formal procedure:

1. Choose a test object.
2. Choose a start configuration of detectors.
3. Simulate measurements for this configuration and reconstruct the object from these "measurement" data.
4. Choose additional test points on the boundary between the detectors and simulate measurement for these points.
5. Test if the simulated output flux of the reconstructed object is well fitted to the "measurement" in the test points too. If not, modify detector arrangement and go to 3.
6. end

Figure 5 shows another correction of the detector arrangement and the corresponding reconstruction result. Now the behaviour of the deviation curves in the test points is very similar to that in the detector points (Fig. 5 left). It is not to be expected that more detectors would provide additional information and improve the reconstruction results.

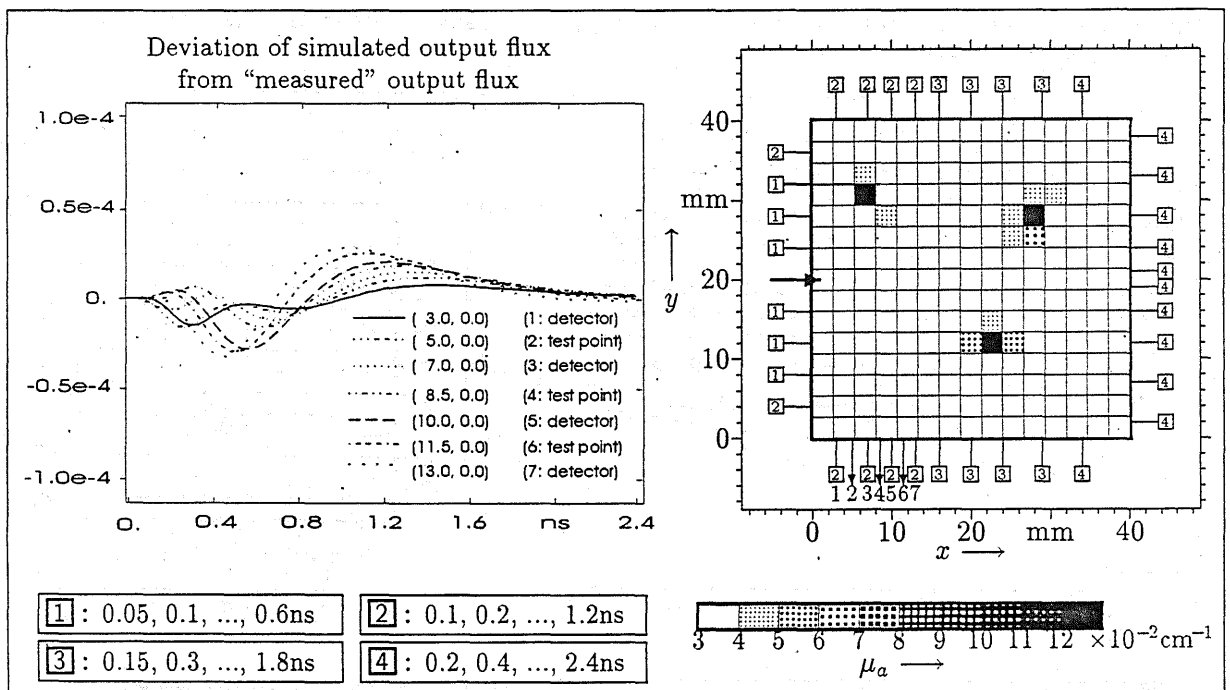


Figure 5: Arrangement (C) of detectors and reconstruction result after 6 iterations.

The right sides of Figures 4 and 5 (arrangements (B) and (C)) show the detectors for only one of the four sources. However, the arrangement in relation to each source is the same. Application of such a method requires the investigation of the output flux for all detectors and test points for each source and various objects in order that a configuration is obtained, which is independent of a specific object. However, it is worthwhile for a final diagnostic measurement configuration.

A similar procedure had to be followed with the sources to get an optimal measurement configuration. Contrary to the increase in the number of detectors, the addition of a source leads to a considerable growth of the computation time. However, an analogous procedure could be applied to the sources.

The improved measurement configuration (C) was used to reconstruct a more complicated structure of absorbers (Fig. 6), which could hardly be detected when only configuration (A) was used.

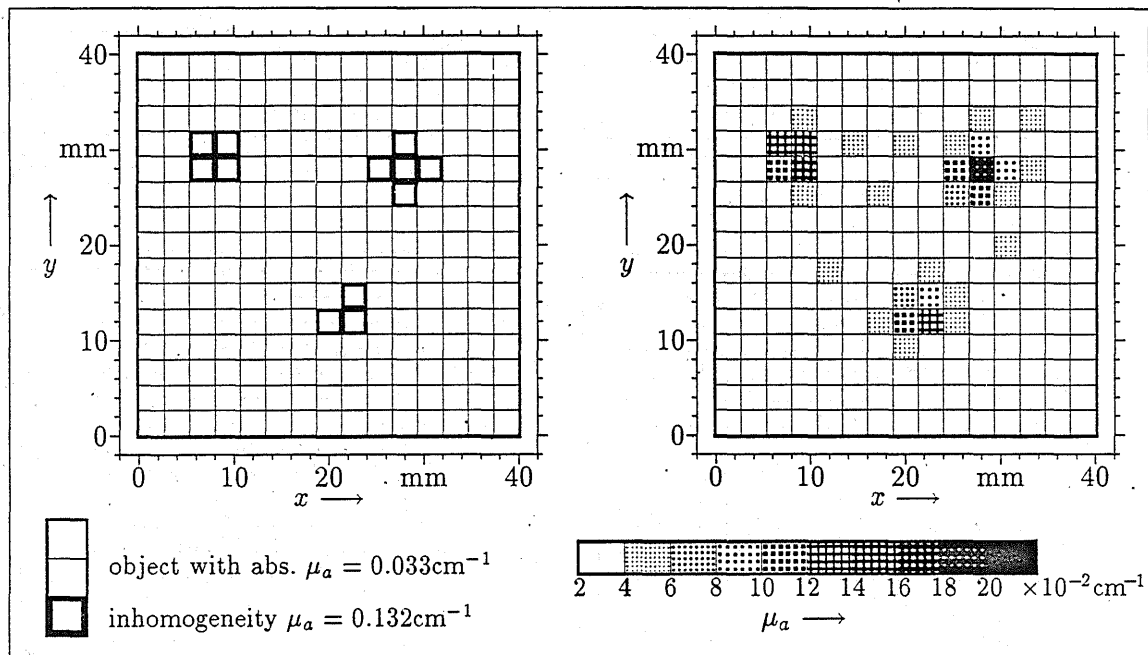


Figure 6: Object (left) and reconstruction result after 6 iterations (right).

3.3 Improvement of the results using Tikhonov regularization

Regularization is a widely used stabilization strategy for algorithms handling ill-conditioned problems. Here, the actual problem is replaced by a better conditioned problem which approximates the original problem if some additional regularization parameters tend to zero. The well-known Tikhonov regularization can be considered as the addition of penalty terms to the error function (6)

$$F(\mu_a, \mu'_s) = \|J^{sim}(\mu_a, \mu'_s) - J^{mes}\|^2 + \beta_a \|\mu_a\|^2 + \beta_s \|\mu'_s\|^2 \quad (7)$$

Each penalty term contains the norm of the optical parameter which must be reconstructed.

When Tikhonov regularization is used, the reconstruction results may be considerably improved. Figure 7 shows an example where the measurement data have been simulated using the test object of section 3.2 (compare Figure 2) with a fixed reduced scattering $\mu'_s = 10\text{cm}^{-1}$ and

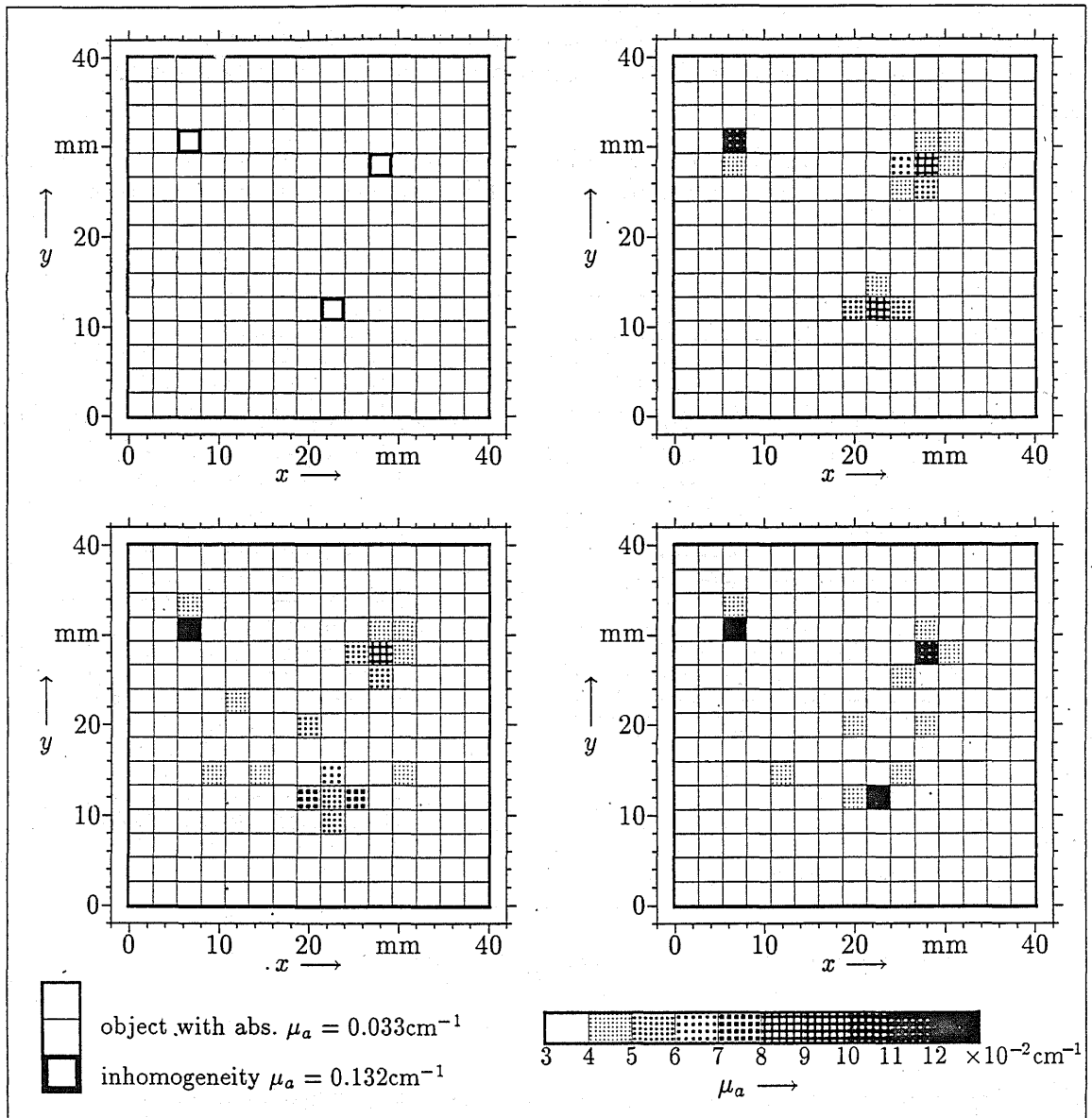


Figure 7: Object with 3 absorbers (top left) reconstruction result after 8 iterations without regularization (top right), with regularization $\beta_a = 10^{-6}$ (left) and $\beta_a = 10^{-7}$ (right).

an underground absorption $\mu_a = 0.033\text{cm}^{-1}$. Unlike the example in section 3.2 (Fig. 3-5), the 3 absorbers shown in Figure 2 had only the 4-fold underground absorption. A comparison of the grey level pictures in Figure 7 shows the effect of the regularization.

The dependence on the appropriate choice of the regularization parameter β_a can be clearly seen. Best results were achieved when the parameter β_a was chosen so that the penalty term and the error function were of the same order of magnitude in the final step of the iteration (5),

$$\beta_a \|\mu_a\|^2 \approx \|\mathbf{J}^{sim}(\mu_a) - \mathbf{J}^{mes}\|^2 \quad (8)$$

In the first tests the regularization parameter was determined from condition (8) using $\|\mu_a\|^2$ and $\|J^{sim}(\mu_a) - J^{mes}\|^2$ of the corresponding unregularized reconstruction result. However, it seems possible to include a strategy into the iteration procedure (5) by which the regularization parameter can be determined automatically.

For the reconstruction of scatterers, β_s is chosen in analogy. An example of the regularization of reduced scattering is given in Figure 8.

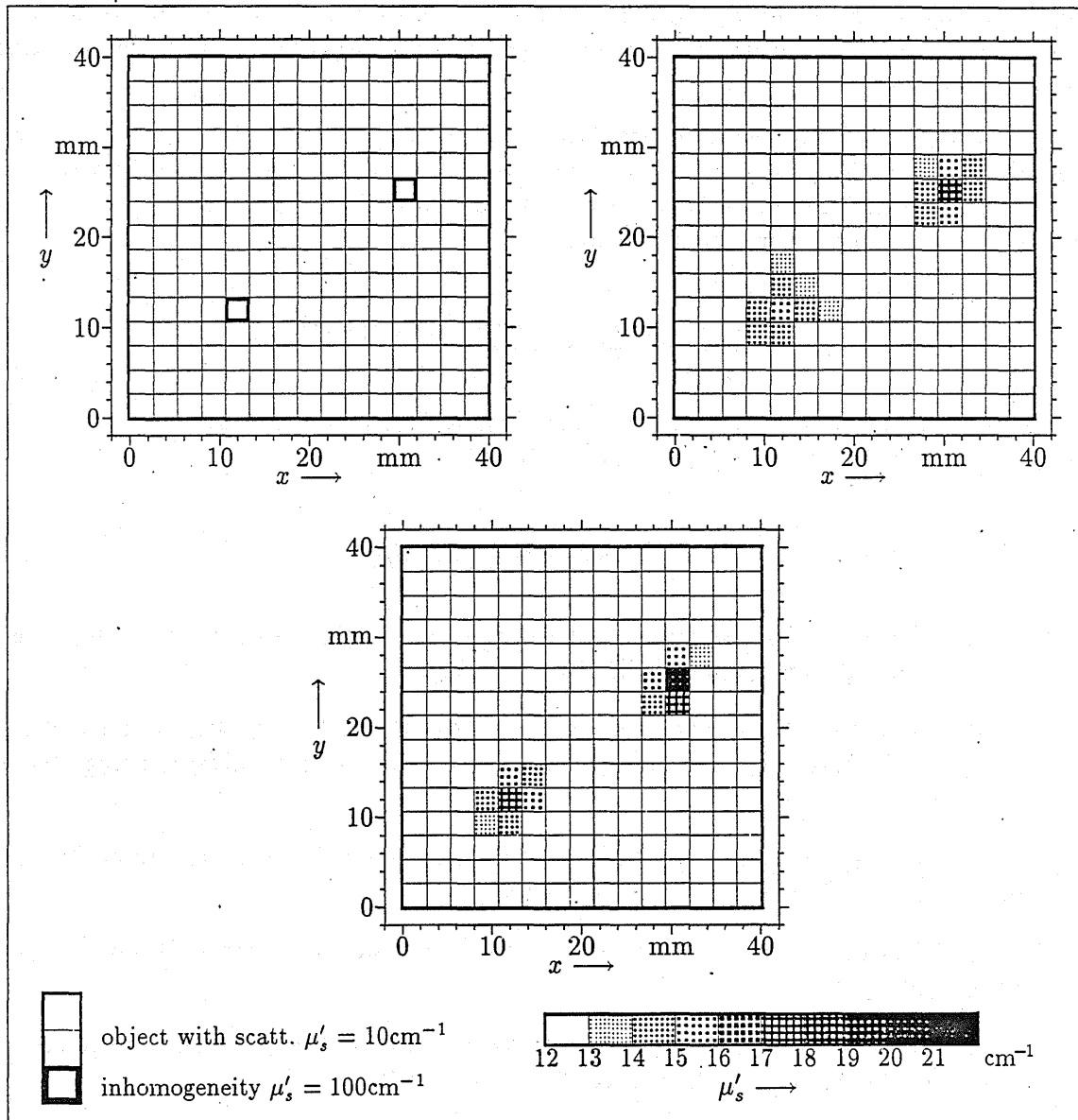


Figure 8: Object (top left) and reconstruction result after 12 iterations without regularization (top right) and with regularization (bottom).

4 CONCLUSIONS

The inverse imaging problem is ill-conditioned. Reconstruction results therefore very sensitively depend both on the measurement data and on the choice of the reconstruction method and the parameters controlling the algorithm. The development of appropriate algorithms makes systematic numerical tests necessary.

The measurement configuration, especially the arrangement of the detectors, has a great influence on the reconstruction result obtained. It is possible to improve the results using appropriate configurations. Regularization methods can improve the reconstruction results or reduce the computation time because of faster convergence. An automatic control of the regularization parameter should be included.

Tests with simulated measurement data are an effective tool for developing and improving reconstruction algorithms. In a next step, the measurement simulation should be more realistic, for example by addition of an artificial noise to the data. The test results achieved encourage us to also take real measurements into consideration.

ACKNOWLEDGEMENTS

This work was supported by the German Federal Ministry of Education, Science, Research and Technology (BMBF), project number 13N6307.

REFERENCES

- [1] S. R. ARRIDGE, The forward and inverse problems in time-resolved infra-red imaging. In Medical optical tomography, SPIE Vol. IS (1993).
- [2] S. R. ARRIDGE, M. SCHWEIGER, M. HIRAOKA, D. T. DELPY, Performance of an iterative reconstruction algorithm for near-infrared absorption and scatter imaging. Proc. SPIE 1888, 360-371 (1993).
- [3] J. E. DENNIS, JR., R. B. SCHNABEL, Numerical Methods for Unconstraint Optimization and Nonlinear Equations. New Jersey (1983).
- [4] C. W. GROETSCH, Inverse Problems in the Mathematical Sciences. Braunschweig/Wiesbaden (1993).
- [5] J. C. HEBDEN, R. A. KRUGER, K. S. WANG, Time-resolved imaging through a highly scattering medium. Appl. Optics 28, 788-794 (1991).
- [6] A. ISHIMARU, Wave propagation in random scattering media. New York (1978).
- [7] F. LIU, K. M. YOO AND R. R. ALFANO, How to describe the scattered ultrashort laser pulse profiles measured inside and at the surface of a random medium using the diffusion theory. Proc. SPIE 1888, 103-106 (1993).

- [8] R. MODEL, R. HÜNLICH, D. RICHTER, H. RINNEBERG, H. WABNITZ, M. WALZEL, Imaging in Random Media: Simulating Light Transport by Numerical Integration of the Diffusion Equation. Proc. SPIE **2326**, 11-22 (1995).
- [9] R. MODEL, R. HÜNLICH, M. ORLT, M. WALZEL, Image reconstruction for random media by diffusion tomography. Proc. SPIE **2389**, 400-410 (1995).
- [10] R. MODEL, R. HÜNLICH, Parameter sensitivity in near infrared imaging. This volume.
- [11] M. S. PATTERSON, B. CHANCE, B. C. WILSON, Time-resolved reflectance and transmittance for the noninvasive measurement of tissue optical properties. Appl. Optics **28**, 2331-2336 (1989).
- [12] J. R. SINGER, F. A. GRUNBAUM, P. KOHN, J. P. ZUBELLI, Image reconstruction of the interior bodies that diffuse radiation. Science **248**, 990-993 (1990).
- [13] Y. WANG, J. CHANG, R. ARONSON, R. L. BARBOUR, H. L. GRABER, J. LUBOWSKY, Imaging of scattering media by diffusion tomography: an iterative perturbation approach. Proc. SPIE **1641**, 58-71 (1992).

Recent publications of the Weierstraß-Institut für Angewandte Analysis und Stochastik

Preprints 1995

175. Alexander A. Gushchin: On efficiency bounds for estimating the offspring mean in a branching process.
176. Vladimir G. Spokoiny: Adaptive hypothesis testing using wavelets.
177. Vladimir Maz'ya, Gunther Schmidt: "Approximate approximations" and the cubature of potentials.
178. Sergey V. Nepomnyaschikh: Preconditioning operators on unstructured grids.
179. Hans Babovsky: Discretization and numerical schemes for stationary kinetic model equations.
180. Gunther Schmidt: Boundary integral operators for plate bending in domains with corners.
181. Karmeshu, Henri Schurz: Stochastic stability of structures under active control with distributed time delays.
182. Martin Krupa, Bjn Sandstede, Peter Szmolyan: Fast and slow waves in the FitzHugh–Nagumo equation.
183. Alexander P. Korostelev, Vladimir Spokoiny: Exact asymptotics of minimax Bahadur risk in Lipschitz regression.
184. Youngmok Jeon, Ian H. Sloan, Ernst P. Stephan, Johannes Elschner: Discrete quadrature methods for logarithmic–kernel integral equations on a piecewise smooth boundary.
185. Michael S. Ermakov: Asymptotic minimaxity of chi-square tests.
186. Björn Sandstede: Center manifolds for homoclinic solutions.
187. Steven N. Evans, Klaus Fleischmann: Cluster formation in a stepping stone model with continuous, hierarchically structured sites.
188. Sybille Handrock–Meyer: Identifiability of distributed parameters for a class of quasilinear differential equations.

189. James C. Alexander, Manoussos G. Grillakis, Christopher K.R.T. Jones, Björn Sandstede: Stability of pulses on optical fibers with phase-sensitive amplifiers.
190. Wolfgang Härdle, Vladimir G. Spokoiny, Stefan Sperlich: Semiparametric single index versus fixed link function modelling.
191. Oleg Lepskii, Enno Mammen, Vladimir G. Spokoiny: Optimal spatial adaptation to inhomogeneous smoothness: An approach based on kernel estimates with variable bandwidth selectors.
192. William McLean, Siegfried Prößdorf: Boundary element collocation methods using splines with multiple knots.
193. Michael H. Neumann, Rainer von Sachs: Wavelet thresholding in anisotropic function classes and application to adaptive estimation of evolutionary spectra.
194. Gottfried Bruckner, Siegfried Prößdorf, Gennadi Vainikko: Error bounds of discretization methods for boundary integral equations with noisy data.
195. Joachim Förste: Das transversale Feld in einem Halbleiterinjektionslaser.
196. Anatolii Puhalskii, Vladimir G. Spokoiny: On large deviation efficiency in statistical inference.
197. Klaus Fleischmann, Carl Mueller: A super-Brownian motion with a locally infinite catalytic mass.
198. Björn Sandstede: Convergence estimates for the numerical approximation of homoclinic solutions.
199. Olaf Klein: A semidiscrete scheme for a Penrose-Fife system and some Stefan problems in \mathbb{R}^3 .
200. Hans Babovsky, Grigori N. Milstein: Transport equations with singularity.
201. Elena A. Lyashenko, Lev B. Ryashko: On the regulators with random noises in dynamical block.
202. Sergei Leonov: On the solution of an optimal recovery problem and its applications in nonparametric statistics.
203. Jürgen Fuhrmann: A modular algebraic multilevel method.